GENERATING ELECTRIC POWER WITH A MEMS ELECTROQUASISTATIC INDUCTION TURBINE-GENERATOR

J.L. Steyn[1], S.H. Kendig[1], R. Khanna[1], T.M. Lyszczarz[2], S.D. Umans[1], J.U. Yoon[2]*
C. Livermore[1], J.H. Lang[1]
[1]Massachusetts Institute of Technology, Cambridge, Massachusetts, USA
[2]Lincoln Laboratory, Massachusetts Institute of Technology, Lexington, Massachusetts, USA

Abstract

This paper presents a microfabricated electroquasistatic (EQS) induction turbine-generator that has generated net electric power. A maximum power output of 192 μW was achieved under driven excitation. We believe that this is the first report of electric power generation by an EQS induction machine of any scale found in the open literature. This paper also presents self-excited operation in which the induction generator self-resonates and generates power without the use of any external drive electronics. The generator comprises five silicon layers, fusion bonded together at 700^{o}C. The stator is a platinum electrode structure formed on a thick (20 μm) recessed oxide island. The rotor is a thin film of lightly doped polysilicon also residing on an oxide island, (10 μm) thick. This paper also presents a generalized state-space model for an EQS induction machine that takes into account the machine and its external electronics and parasitics. This model correlates well with measured performance and was used to find the optimal drive conditions for all driven experiments.

1 Introduction

Batteries have been, and still remain, the energy storage medium of choice for many portable electric and electronic applications. Most hydrocarbon fuels have energy densities that are approximately $20-30$ times greater than most batteries and therefore present an attractive alternative, provided that a means can be found to convert the enthalpy of combustion of a hydrocarbon fuel into electric power. On the macroscale, gas turbine (Brayton) cycles can have high efficiencies, and turbomachines lend themselves to reliable continuous operation for long periods of time. Research at MIT focuses on the development of a miniaturized gas turbine generator to deliver $1-50$ W of electric power [1].

In MIT's device, a small gas turbine engine provides the shaft power needed to drive a small electric generator. Presented here is an electroquasistatic (EQS) induction generator for the microengine. Although magnetic machines are preferred at large scales, EQS machines become attractive at small scales, primarily because very small airgaps between the rotor and stator allow higher breakdown electric fields of order 10^8 V/m. Macroscale EQS motors have been reported previously, but even relatively small conventionally fabricated devices (e.g. [2,3]) perform rather poorly compared to their magnetic counterparts. Previously at MIT, Nagle [4], Fréchette [5], and Livermore [6] presented microfabricated EQS induction micromotors. The device in [6] attained a maximum speed of 55 krpm, a maximum torque of 3.5 μNm and a maximum airgap power of 20 mW, the highest airgap power of any MEMS micromotor to date. Attempts to produce an EQS induction generator have, until now, not been successful [7].

*Corresponding author: J.L. Steyn (lodewyk@alum.mit.edu)

2 Device layout and operation

Figure 1 describes the essence of an EQS induction machine. Every 6$^{\text{th}}$ stator electrode is connected to form a six-phase machine. Sinusoidal voltages on the six phases, phased 60 degrees apart, produce the traveling stator wave. The rotor in this machine is a high resistivity polysilicon film that causes the rotor potential to lag or lead the stator potential. The traveling potential wave on the stator induces a traveling potential wave on the rotor. If the rotor spins slower than the rotor potential wave, the machine operates as a motor. If the rotor spins faster, as depicted in Figure 1, it operates as a generator.

The actual device is shown in schematic 3D cross-section in Figures 2 and 3. The device structure is similar to devices presented earlier [4–6]. In Figure 2, the first layer, L1, forms the structural support and provides connections for the turbine main air and front thrust bearing. Layer L2 is a distribution manifold. The turbine rotor and stator blades are formed on the top side of L3. The bottom of L3 has the rotor film for the induction machine on top of a thick (10 μm) oxide island. L4 is the stator, with 786 platinum electrodes arranged in 131 interleaved groups of 6 electrodes. L5 is the lower structural layer that provides air connections for the rear thrust bearing and the journal bearing of the turbine. Figure 4 is a picture of the actual device.

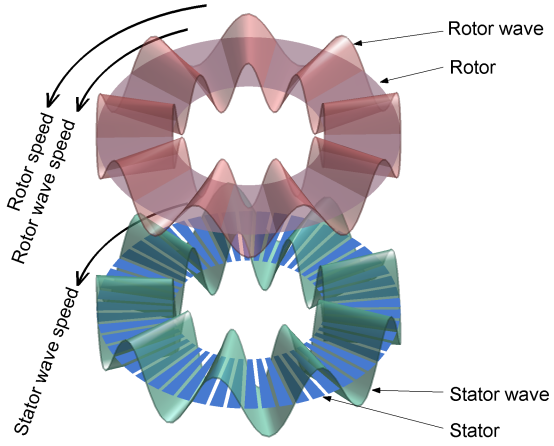

Figure 1: The essence of an EQS induction machine. A basic 6-phase machine consists of a stator with a set of electrodes arranged such that every 6th electrode is connected. Sinusoidal voltages on the six electrode sets, phased 60 degrees apart, produce a traveling wave. This in turn induces a traveling potential wave on the rotor—a high resistivity polysilicon film in this case.

3 Device modeling

Figure 5 is a model of the machine attached to its external circuitry. This is a resonant system that can excite itself and is a

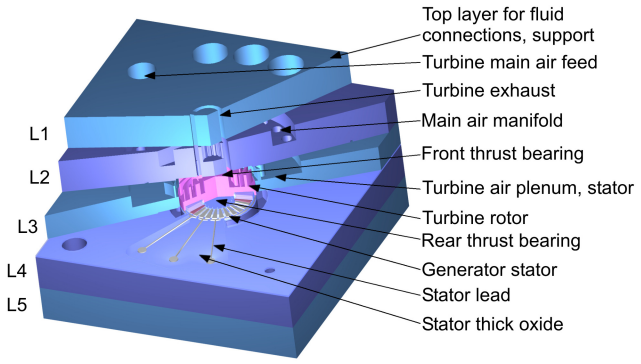

Figure 2: 3D section view of the turbine generator device

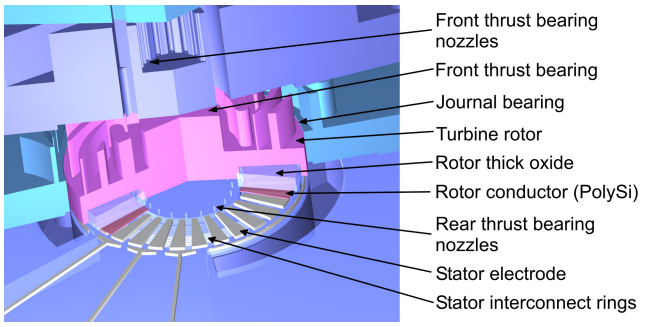

Figure 3: Detail of the rotor-stator structure. The stator periodicity is reduced for visual clarity. The actual stator has 786 electrodes.

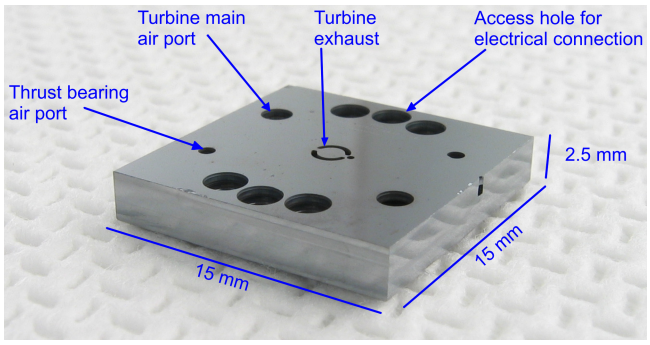

Figure 4: Photograph of the generator device

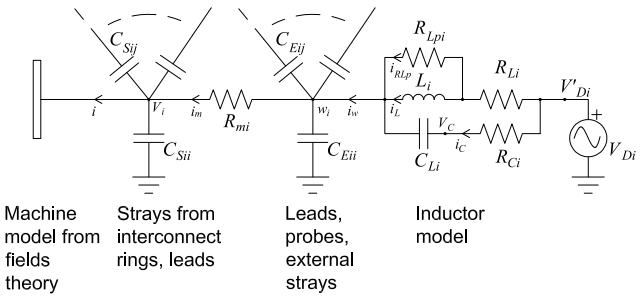

Figure 5: Circuit description of the generator and its inductors. The machine model on the left takes into account any inter-phase capacitive coupling internal to the machine.

substantial improvement on earlier models. Work by Bart [8] and Nagle [4] addressed mainly the rotor and stator fields analyses and assumed balanced operation in which all the phases were identical. In Figure 5 the machine model is obtained in similar fashion from EQS field theory. This, however, is a general polyphase model for the i^{th} phase of the generator. C_{Sij} and C_{Eij} are components of the general, non-symmetric stator and external capacitance matrices. Each of the six inductors attached to the machine is independently modeled to include core, wiring and wire insulation dielectric losses. Subscripts i and j refer to phases 1 through 6. This model accurately and successfully guided the experiments, as described below, and helped to determine the optimal drive voltages and phase angles V_{Di}, $i \in \{1,2,3,4,5,6\}$, whenever a driven excitation was used.

4 Fabrication

The generator is fabricated using a combination of standard IC fabrication techniques, deep reactive ion etching (DRIE), and multi-wafer bonding. Its fabrication is similar to that described in [5]. The deep, high aspect ratio etch of the journal bearing in L3 is challenging [9], and is required to be $20 \pm 1\,\mu$m wide and $300\,\mu$m deep. Good control of the journal bearing fabrication enables rotational speeds of up to 850 krpm to be reached. Thick oxide layers are required in Layers 3 and 4 to minimize capacitive coupling to the rotor and stator backplanes. To minimize wafer bow, the insulator oxide is limited to island areas where needed. The rotor oxide is a $10\,\mu$m thick PECVD film, and the stator oxide a $20\,\mu$m PECVD TEOS film. The stator fabrication process is described further in [6]. The bond between L3 and L4 is a fusion bond between PECVD oxide and silicon. The PECVD oxide is smoothed by repeated oxide deposition and CMP until a bondable surface is obtained with a test wafer. After smoothing, L4 is annealed at 750°C for 3 hours to allow for outgassing of the PECVD oxide prior to bonding. Only then does fabrication of L4 proceed as before. The bondability verification procedure with known good blank wafers, combined with rework where needed, enables the bonding of a 5-layer wafer stack with 100% bond yield. The final room temperature bonded stack is room-temperature pressed with a uniform load of 3 kN for 24 hours, then placed under a uniform thermal press of 3 kN for 4 h at 500°C, and finally annealed at 700°C for 22.5 hours.

5 Device Characterization

To excite the six-phase generator, 6 voltages (V_{Di} in Figure 5), along with 5 phases, the frequency and the speed, must be specified. The generated power will depend on all 13 of these parameters. Finding the optimal operating point experimentally is impractical, and a model-guided, computer-optimized approach is preferred. This requires an accurate model. Therefore, the model described in Section 3 must be calibrated to the actual machine and its experimental setup to be useful. The machine was characterized using a frequency domain method. The generator was run at 50 krpm. Each phase (V_{Di}) of the machine was in turn swept in frequency and the other phases were grounded. The voltages w_i (magnitude and phase) were recorded for all six phases. This experiment was repeated six times, to give six datasets, each with a magnitude and phase response for all six phases, and therefore 36 frequency response functions (FRF's). The model was then compared to the experimental data, and a nonlinear least squares algorithm was used to adjust the external capacitance matrix C_{Eij}, the gap G and the rotor conductivity σ_s to best fit the data. Figure 6 shows the FRF for the case where Phase 1 was the driven phase, and all the others were grounded, to-

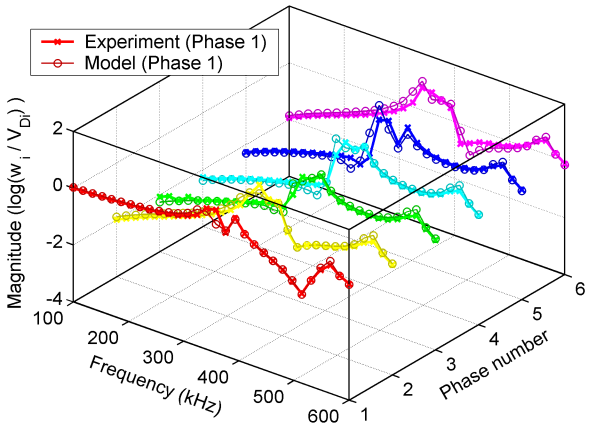

Figure 6: Frequency response of all the phases under Phase 1 excitation.

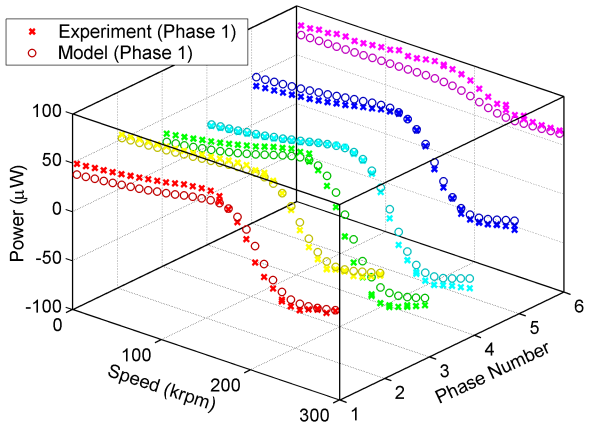

Figure 7: Individual per phase powers versus mechanical speed. Negative power indicates power generated, according to the sign convention that power entering the device is positive.

gether with the model result after fitting. Typical values for $C_{\mathrm{Eij}}, i = j$ and $C_{\mathrm{Eij}}, i \neq j$ were 4.5 pF and 0.5 pF respectively. For the gap and the rotor conductivity, values of $G = 4.2\,\mu$m and $\sigma_s = 0.75$ nS were obtained.

6 Experiments under driven excitation

Driven excitation experiments were first performed on the EQS generator. Under these conditions, the V_{Di}'s in Figure 5 were applied with six function generators (Agilent 33220A), one for each phase. A 1 kΩ current sense resistor was placed in series with the voltage sources. The per phase real and reactive powers were measured with six Analog Devices AD835 multipliers at points V'_{Di}. The inductors for this application were JW Miller Model 4671 inductors with a nominal inductance of $L = 8.2$ mH. For these inductors, the following were measured to be the nominal model parameters: $C_L = 1.7$ pF, $R_L = 40\,\Omega$, $R_{Lp} = 1\,\mathrm{M}\Omega$, $R_C = 1\mathrm{k}\Omega$. (See Figure 5.)

To further reduce the capacitive loading on the device and make net generation possible, the voltage probes (Agilent 10440B 100:1 probes, 2.5 pF||10 MΩ) used to measure w_i during device characterization were removed for this experiment. Therefore, $C_{Eij}, i = j$ was reduced from approximately 4.5 pF to 2 pF per phase.

With the new C_{Eij} matrix, a nonlinear optimization was performed on the model to find the power-optimal drive voltages and phases, as well as the optimal speed and electrical frequency. All voltage magnitudes converged to their upper bounds for most optimizations. Without these optimizations it was nearly impossible to determine an operating point that produced net power generation.

Figure 7 shows the per phase power-speed relationship obtained when exciting the machine with $V_{Di} = 1.6\,\mathrm{V_{pp}}$, and phase angles $0, -30.4, -110.1, -195.7, -217.7, -254.6$ degrees, at 402.9 kHz. The curve in Figure 8 is the real power sum of all the phases. A maximum of 108 μW at 245 krpm was generated in this experiment. Good correlation with the model was observed.

Because the model is accurate, it can be used to estimate the power lost in various parts of the turbine-generator system. At 245 krpm a total of approximately 300 mW enters the turbine in the airstream. Turbine inefficiencies dissipate 219 mW. This is understandable, given that the design speed of the turbine is 2.4 Mrpm. A further 54 mW is dissipated in airgap viscous losses, with 26.7 mW accounting for journal and thrust bearing viscous losses. A negative torque of 0.03 μNm

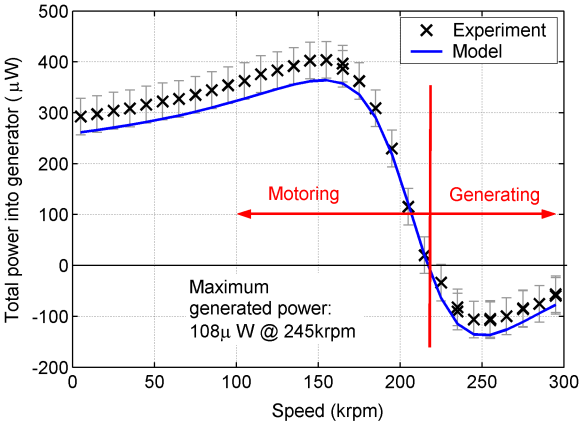

Figure 8: Sum of the per phase powers versus mechanical speed. Negative power indicates power generated, according to the sign convention that power entering the device is positive.

is produced by the airgap electric fields, corresponding to a mechanical power input to the generator of 790 μW. Of this shaft power, 255 μW is lost in the rotor conductor and 535 μW enters the external circuit depicted in Figure 5. Internal machine interconnect and wiring resistances account for 75 μW of the losses. The bulk of the power from the machine, 280 μW, is dissipated in the inductor core, with inductor wiring and dielectric and proximity losses accounting for 50 μW and 22 μW respectively. The airflow to electric efficiency of the device is 0.036% and the mechanical to net electrical efficiency is 14%.

Other experiments at excitation voltages as high as $3\,\mathrm{V_{pp}}$ were also performed. In these experiments, correlation to the linear model presented in this paper was not as good, due to a nonlinearity in the rotor conductor film. The maximum power output of the generator to date was 192 μW, recorded at an excitation voltage of $V_{Di} = 2.4\,\mathrm{V_{pp}}$.

7 Experiments under self-excitation

Under self excitation, the sources V_{Di} were set to zero and the mechanical speed was increased. In this experiment the voltage w_4 on Phase 4 was measured using a capacitive divider. At speeds greater than 215 krpm the machine self-excited. A maximum voltage of approximately $40\,\mathrm{V_{pp}}$ was measured at 411 kHz. This eigenfrequency was within 1 kHz of the eigen-

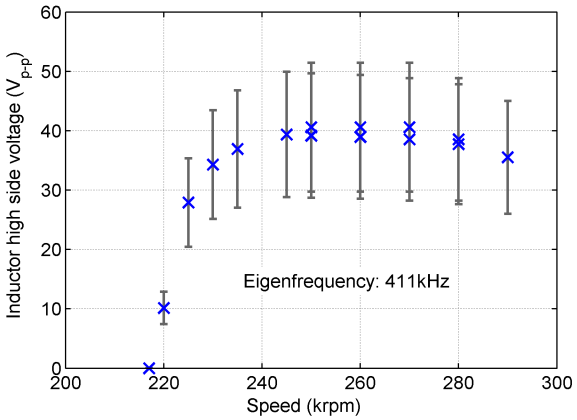

Figure 9: Results from the self-excitation experiments. Shown here is the peak-to-peak voltage at w_4, the inductor high side on Phase 4, as a function of the rotational speed. At speeds greater than 215 krpm *the device self-excites.*

frequency predicted by the model presented earlier. All the power generated by the EQS generator was dissipated in the wiring resistances and in the inductors.

A nonlinearity in the rotor conductor limited the machine output in this experiment. The rotor electric fields in the direction of rotation can reach approximately $1-10\,\mathrm{kV/cm}$. At these fields, carrier drift saturation becomes important [10]. Tests are underway to better determine the high field properties of these Boron-doped polysilicon rotor conductor films.

8 Summary and conclusions

The results reported here demonstrate the feasibility of an electroquasistatic induction micromachine as a generator. The amount of power it can generate is limited by its external and internal stray capacitances. It is therefore necessary to minimize all the strays and accurately model those that remain along with their imbalance. Inductor modeling must also be accurate over a wide frequency range. The total model may then be used to guide generator operation. This paper demonstrates that it is possible to estimate the external strays and other parameters—in this case a total of 23—from a suitable set of frequency domain experiments using a nonlinear least squares technique. The calibrated models are in agreement with the measured results and can be used with confidence to design future devices of this kind.

The device presented here was operated over a speed range of $200-300\,\mathrm{krpm}$ and a drive voltage range of $V_{\mathrm{Di}} = 0-3\,\mathrm{V_{pp}}$. The maximum power recorded was $192\,\mu\mathrm{W}$. At $V_{\mathrm{Di}} = 1.6\,\mathrm{V_{pp}}$, $108\,\mu\mathrm{W}$ was produced and the machine terminal voltages w_i were $\sim 30\,\mathrm{V_{pp}}$. At the terminals, $535\,\mu\mathrm{W}$ was generated. Scaling to design conditions, using the linear model and assuming a better rotor conductor can be found, it is predicted that with a terminal voltage of $600\,\mathrm{V_{pp}}$, at 900 krpm, this device could produce 0.5 W at the terminals.

The possibility of self-excitation, without the need for external drive electronics, greatly simplifies the practical implementation of power generation applications. At both high driven voltages ($w_i \approx 50\,\mathrm{V_{pp}}$) and under self-excited operation, a significant power-limiting nonlinearity was identified and experiments are underway to better characterize it.

Power generation could only be attained at high operating speeds ($> 200\,\mathrm{krpm}$) with a generator that used a metal stator for minimal stator resistive loss. Our generator addressed these requirements by being the first fully-bonded MEMS EQS induction machine with a metal stator structure. This stator structure had a PECVD oxide surface as a bond surface, where surface bondability was achieved after the fabrication of that layer. A precise, $20\,\mu$m wide, $300\,\mu$m deep journal bearing allowed for stable operation beyond the synchronous speed.

Acknowledgments

Chiang Juay Teo operated the spinning generator at speeds up to 850 krpm. Gwen Donahue contributed to the journal bearing process development. Crystal Law provided the 3D solid models and rendering under the MIT UROP program. All microfabrication was performed at the MIT Microsystems Technology Laboratories (MTL) and at the Micro Electronics Laboratory (MEL) at MIT Lincoln Laboratory. Lodewyk Steyn was supported in part by an Applied Materials Graduate Fellowship. Both Sam Kendig and Crystal Law were supported by the Reed Fund. The work at Lincoln Laboratory was sponsored by the Defense Advanced Research Projects Agency under Air Force Contract F19628-00-C-0002. Funding for the development of microengine technology was provided by the Army Research Laboratory (DAAD19-01-2-0010) under the Collaborative Technology Alliance in Power and Energy program, managed by Mr. John Hopkins (ARL) and Dr. Mukund Acharya (Honeywell), and by the Army Research Office (DAAG55-98-1-0292) managed by Dr. Tom Doligalski. Opinions, interpretations, conclusions, and recommendations are those of the authors and are not necessarily endorsed by the United States Government.

References

[1] Epstein, A.H., "Millimeter Scale MEMS Gas Turbine Engines", Proc. of ASME Turbo Expo 2003, Power for Land, Sea, and Air, June 16-19, 2003, Atlanta, Georgia, USA

[2] Mognaschi, E.R., Calderwood, J.H, "Asynchronous dielectric induction motor", Science, Measurement and Technology, IEE Proceedings A , Volume: 137 , Issue: 6 , Nov. 1990.

[3] Bollée, B., "Electrostatic motors", Philips Technical Review, 30 (6/7), 1969, 178-94

[4] Nagle, S.F., "Analysis, Design and Fabrication of an Electric Induction Micromotor for a Micro Gas-Turbine Generator", Ph.D. Thesis, MIT, 2001.

[5] Fréchette, L. et al, "An Electrostatic Micromotor Supported on Gas-Lubricated Bearings", MEMS 2001, Interlaken, Switzerland, January 2001.

[6] Livermore, C. et. al, "A High Power MEMS Electric Induction Motor", J. MEMS, V30, No. 3, June 2004

[7] Willke, T.L., "Self-excited Electrostatic Generator", M.S. Thesis, MIT, 1968

[8] Bart, S.F., Lang, J.H., "An Analysis of Electroquasistatic Induction Micromotors", Sensors and Actuators, 20, 1989, 97-106

[9] Li, H.Q. et. al, "Fabrication of a High Speed Microscale turbocharger", Proc. Hilton Head Solid State Sensor, Actuator and Microsystems Workshop, Hilton Head, SC, USA, June 2004.

[10] Sze, S.M., "Semiconductor Devices, Physics and Technology", Wiley, 1986